Energy Conversion and Management 122 (2016) 182–194

Contents lists available at ScienceDirect

Energy Conversion and Management

journal homepage: www.elsevier.com/locate/enconman

Optimal economic and environment operation of micro-grid power systems

Moataz Elsied *, Amrane Oukaour, Hamid Gualous, Ottavio A. Lo Brutto

University of Caen Basse Normandie, LUSAC Laboratory, Caen, France

ARTICLE INFO

Article history:
Received 19 January 2016
Received in revised form 23 May 2016
Accepted 25 May 2016

Keywords:
Distributed Energy Resources (DERs)
Micro-grid (MG)
Energy Management System (EMS)
Binary Particle Swarm Optimization (BPSO)

ABSTRACT

In this paper, an advanced real-time energy management system is proposed in order to optimize micro-grid performance in a real-time operation. The proposed strategy of the management system capitalizes on the power of binary particle swarm optimization algorithm to minimize the energy cost and carbon dioxide and pollutant emissions while maximizing the power of the available renewable energy resources. Advanced real-time interface libraries are used to run the optimization code. The simulation results are considered for three different scenarios considering the complexity of the proposed problem. The proposed management system along with its control system is experimentally tested to validate the simulation results obtained from the optimization algorithm. The experimental results highlight the effectiveness of the proposed management system for micro-grids operation.

1. Introduction

Recently, there is a great interest in using micro-grids (MGs) in power systems as they are considered flexible, intelligent, and active power network [1]. In addition, they are able to improve system reliability, efficiency, and security leading to more promotion of the renewable energy sources integration [2]. MGs can either be connected to the grid (i.e., grid-connected mode) or use the Distributed Energy Resources (DERs) to supply the loads without the grid (i.e., islanded mode) [3].

For MGs context, Energy Management System (EMS) plays an important role in the power systems' operation [4]. The concept of Micro-Grid Energy Management Systems (MGEMS) based on Unit Commitment (UC) and Optimal Power Flow (OPF) models have been reported in details in the literature.

In [5], a UC based on multi-objective energy management system is proposed in order to optimize micro-grid performance considering the operational constraints and the existence of three different types of customers. A UC based on a robust EMS is introduced in [6] for a CHP micro-grid considering the uncertainty of electricity demands, heat demands and electricity price. In [7], a UC based EMS is proposed to determine optimal dispatch of micro-grid based on photovoltaic system, batteries and ultra-capacitors with the objective of optimum power charging or discharging for Energy Storage Systems (ESS) in order to avoid overcharges and discharges.

On the other hand, the OPF based EMS models is introduced in [8] for solar photovoltaic-diesel-battery hybrid power supply system for off-grid applications. The aim was to meet the load demand completely while satisfying the system constraints taking into account photovoltaic power availability, battery bank state of charge and load power demand. In [9], an OPF based EMS for industrial micro-grids working in grid connected mode is proposed considering constraints associated with power flows, ESS, and plug-in electric vehicles.

Summarily, the objectives of MGEMS are identified in [10] as controlling frequency and voltage as well as improving the power quality through unbalance and harmonics mitigation. In [11], the objectives are introduced as insuring power balance between generation and demand, reducing the operating cost and minimizing the emission level. In [12], the objectives are presented as obtaining optimal control for the micro-grid operation, lowering risk of total system break-down and increasing the power system efficiency.

Various efficient optimization algorithms have been considered in the literature to solve the optimization problems of MGEMS. In [13], the evolutionary optimization algorithm is proposed to minimize the sum of the total capital, operational and maintenance cost of DERs subject to constraints such as energy and emission limits of each DER and Loss of Power Supply Probability (LPSP) of MGs. Ant Colony Optimization (ACO) is used in [14] to solve the economic and environmental dispatch of MGs containing different

* Corresponding author at: University of Caen Basse Normandie, LUSAC Laboratory, BP78 Rue Louis Aragon, 50130 Cherbourg, France.
E-mail address: ELSIED_M@esiee-amiens.fr (M. Elsied).

http://dx.doi.org/10.1016/j.enconman.2016.05.074
0196-8904/

Nomenclature

ACO	Ant Colony Optimization
AIMMS	advanced integrated multi-dimensional software
ALLC	advanced lead-lag compensator
BPSO	Binary Particle Swarm Optimization
$C_{DERi}(t)$	total operating cost of DERs at hour t (€ct/kW h).
$C_{gr}(t)$	cost of receiving (buying) power from the main grid (€ct/kW h).
$C_{gs}(t)$	cost of sending (selling) power to the grid (€ct/kW h)
$D_{DERi}(t)$	status of DERs (on state = 1/off state = 0).
DERs	distributed Energy Resources
$D_{ESSj}(t)$	status of ESSs (on state = 1/off state = 0).
$E_{CO_2}^{max}$	maximum emission rate of CO2 for each unit in kg at time t.
$E_{CO_{2g}}(t)$	emission factor of carbon dioxide delivered by the utility grid.
$E_{CO_{2DERi}}(t)$	emission factor of carbon dioxide delivered by each DER.
EMS	energy Management System
$E_{NO_X}^{max}$	maximum emission rate of NO_X for each unit in kg at time t.
$E_{NO_{XDERi}}(t)$	emission factor of nitrogen oxides delivered by each DER
$E_{NO_{Xg}}(t)$	emission factor of nitrogen oxides delivered by the utility grid.
$E_{SO_2}^{max}$	maximum emission rate of SO_2 for each unit in kg at time t.
$E_{SO_{2DERi}}(t)$	emission factor of sulfur dioxide delivered by each DER.
$E_{SO_{2g}}(t)$	emission factor of sulfur dioxide delivered by the utility grid.
ESS	energy storage systems
FC	Fuel Cell
GA	Genetic Algorithm
LCOE	Levelized Cost Of Electricity
LPSP	Loss of Power Supply Probability
MGEMS	Microgrid Energy Management System
MGs	Micro-Grids
OPF	Optimal Power Flow
$P_{DERi}(t)$	active output power of DERs at hour t in (kW).
$P_{DERi}^{max}(t)$	maximum operating power of each DER
$P_{DERi}^{min}(t)$	minimum operating power of each DER
PEIC	Power Electronics Interface Circuits
$P_{ESSj}(t)$	ESS charging/discharging power at hour t in (kW).
P_{gr}, P_{gs}	the receiving/sending power from/to the grid at hour t in (kW)
$P_L(t)$	load demand power at hour t (kW)
PV	Photovoltaic
PWM	Pulse Width Modulation
RT-EMS	Real-Time Energy Management System
UC	Unit Commitment
WT	Wind Generator
X	vector of optimization state variables.

types of generation systems. In addition, genetic algorithm (GA) is introduced in [15] to achieve economic operation of MGs taking into account emission constraints. Other than that, an advanced EMS in a typical MG working in grid and island operating mode is introduced in [16] based on Advanced Integrated Multidimensional Modeling Software (AIMMS) to determine the optimal operating strategies by minimizing the energy costs and limiting the pollutant emissions.

However, these methods are often used offline, which restrict their use for real-time applications. Real-Time Energy Management Systems (RT-EMSs) is needed to control an environment by receiving data, processing them, and returning the results sufficiently quickly to affect the environment at that time. Recently, efficient RT-EMSs have been proposed in the literature. In [17], RT-EMS for stand-alone MGs in day-ahead markets is introduced based on local energy market algorithm while in [18] is presented using multi-period gravitational search algorithm. These systems are able to successfully achieve autonomous or grid-connected decision making to determine the hourly optimal dispatch of each DER and ESS unit depending on system constraints and market parameters.

In this regard, this paper presents an advanced RT-EMS for MG systems based on real-time libraries in dSPACE (MLIB/MTRACE) [19]. The novelty of this work is to use these libraries as new tools to exchange the information and decision commands between the RT-EMS, DERs, local controllers, and Power Electronics Interface Circuits (PEICs) in real time environment. The optimization model is solved using Binary particle swarm optimization algorithm (BPSO) which is able to satisfy the load demand requirements during 24 h operation with the lowest utility cost by finding an hourly optimal allocation for each DER unit. The proposed RT-EMS is experimentally tested through three scenarios to validate the obtained results from the optimization algorithm. The simulation and experimental results highlight the effectiveness of the proposed RT-EMS for MGs.

The paper is organized as follows: firstly, the MG system description is illustrated in Section 2. In Section 3, the optimization model and its algorithm are introduced and analyzed. In Section 4, the experimental setup using the proposed RT-EMS with its control system are presented and discussed. Finally, the experimental results are discussed in Section 5.

2. Micro-grid system description

The schematic diagram of the MG under consideration is depicted in Fig. 1. There are three DERs: Photovoltaic (PV), wind generator (WT), and Fuel cell (FC). The integration of DERs is interfaced with the load and the main utility grid by using power electronic converters. Using various energy sources, different power converters topologies are necessary for power flow control to fulfil load power demand requirements. The RT-EMS based on BPSO is introduced to provide each power source by its reference value. It is important to note that the BPSO takes into account the MG system variables, constraints, parameters, cost and emission objective functions. Moreover, it has decision making capabilities for the operation of the MG in grid-connected or islanding mode. In grid-connected mode, unidirectional power is allowed based on market policies. Also, the MG is able to disconnect itself from the main grid if low power quality events occur on the main grid.

In this study, the utility grid is responsible for regulating the DC-link voltage, while other controllable DER units such as FC, PV and WT work in current control mode to regulate their output powers based on the reference signals coming from the RT-EMS and available constraints.

To achieve real-time management, MLIB/MTRACE libraries in dSPACE are used to exchange all information and decision commands between EMS, DERs, local controllers, and PEIC. The role of these libraries will be indicated in the following sections. RT-EMS along with its control system presented in this paper support

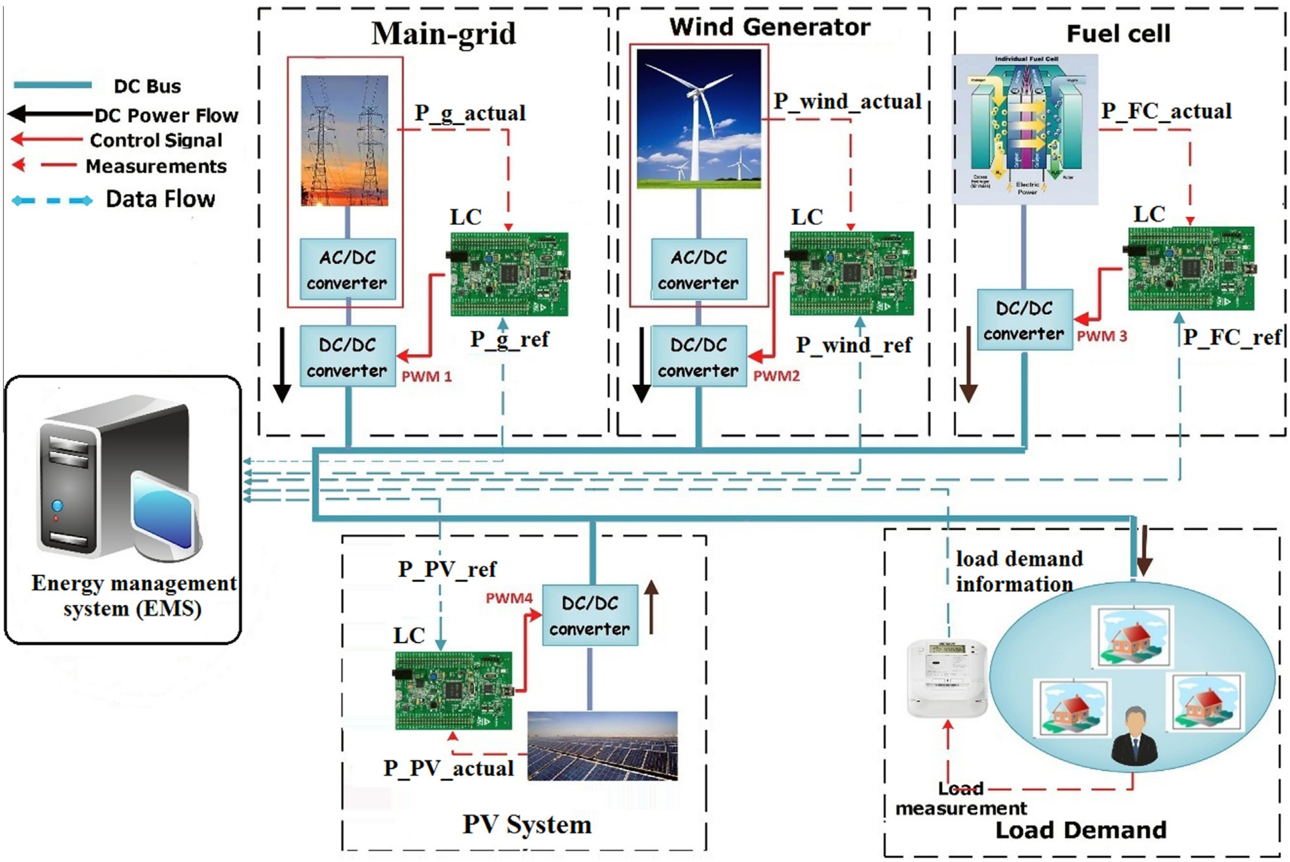

Fig. 1. The schematic diagram of the MG under consideration.

more efficient operation. In addition, it allows a more dynamic, reactive pricing mechanism required to take into account real-time availability of fluctuating DER and follow the evolution of balance between supply and demand in real time.

3. Optimization model

In this section, an optimization model of the RT-EMS is presented. The decision variables include electricity generation of DERs and the main utility grid to allocate each source by its optimal power generation set point. As such, each power source contributes to the load by its optimized rate provided by the RT-EMS. Additionally, energy sources can also be put in ON or OFF state to reach optimal operation of the overall system while satisfying its constraints. The mathematical objective functions are described as follows.

3.1. Proposed objective fitness function

Different cost functions have been already proposed for the literature such as the cost function that presented in [20]. In this paper, a generalized cost function considers the costs of the DERs selling power in addition to the selling and buying costs of exchanging power with the main grid. The main objective of cost function is to supply load demand during the day in an economical manner. Such objective function can be written as:

$$\mathrm{Min} f_1(X) = \mathrm{Min}\sum_{t=1}^{T} cost^t = \mathrm{Min}\sum_{t=1}^{T}\left\{\sum_{i=1}^{u_g} D_{DERi}(t)P_{DERi}(t)C_{DERi}(t) + \sum_{j=1}^{u_s} D_{ESSj}(t)P_{ESSj}(t)C_{ESSj}(t) + P_{gr}(t)C_{gr}(t) - P_{gs}(t)C_{gs}(t)\right\} \quad (1)$$

where $C_{DERi}(t), C_{ESSj}(t)$ are the specific costs of output active power of the ith DERs and jth ESS at hour t. $C_{gr}(t), C_{gs}(t)$ are the costs of receiving (buying)/sending (selling) active power from/to the main grid at hour t. $P_{gr}(t), P_{gs}(t)$ are the receiving/sending active power from/to main grid at hour t, respectively.

In the proposed cost function, $X(1, 2*u*T)$ is considered as the decision variable vector with one row and $(2*u*T)$ columns, consisting of the output power from all DER units and ESS, the amount of exchange power with main utility grid, and on/off mode in a vision planned for the day ahead. This vector can be expressed as follows:

$$X = [P_G, D_G]_{(1,2*u*T)} \quad (2)$$

$$u = \mathrm{ug} + \mathrm{us} + 1 \quad (3)$$

where ug, us are the total number of the DERs and ESS units respectively, T represents the total number of time intervals which is equal to 24 h for one day,P_G is the active power of all DERs and ESS units and D_G is the state vector denoting the ON or OFF states for all DERs and ESS units during each hour of the day. In Eq. (3) the extra number 1 added to the total number of variables u indicates the value of the market production. Each variable in Eq. (2) can be defined as follows:

$$P_G = [P_{DER}, P_{ESS}]$$

$$P_{DER} = \left[P_{DER1}, P_{DER2}, \ldots, P_{DER(ug+1)}\right]$$

$$P_{DERi} = [P_{DERi}(1), P_{DERi}(2), \ldots, P_{DERi}(t), \ldots, P_{DERi}(T)];$$
$$i = 1, 2, \ldots, (ug+1)$$

$$P_{ESS} = \left[P_{ESS1}, P_{ESS2}, \ldots, P_{ESS(us)}\right]$$

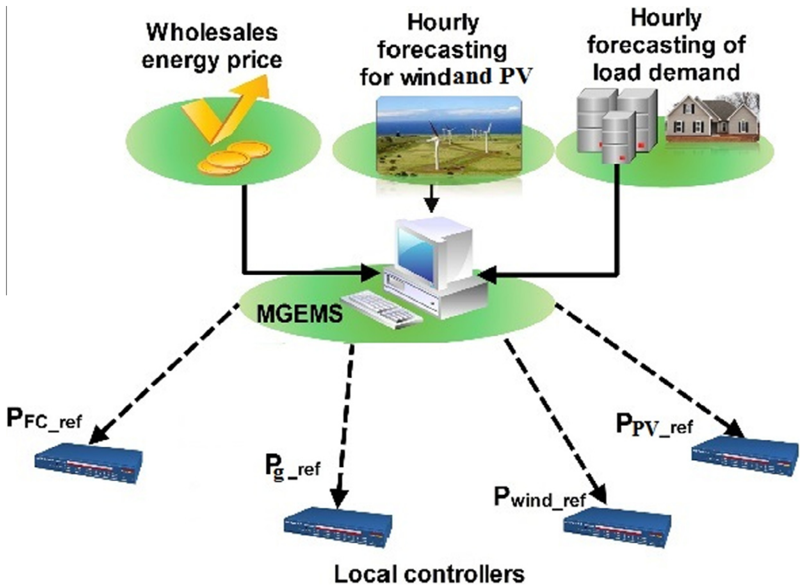

Fig. 2. MG system variables.

$$P_{ESSj} = \left[P_{ESSj}(1), P_{ESSj}(2), \ldots, P_{ESSj}(t), \ldots, P_{ESSj}(T)\right];$$
$$j = 1, 2, \ldots, us \tag{4}$$

where $P_{DERi}(t),\ P_{ESSj}(t)$ are the output active power of the ith DERs and jth ESS units at hour t.

$$D_G = [D_{DER}, D_{ESS}]$$

$$D_{DER} = \left[D_{DER1}, D_{DER2}, \ldots, D_{DER,(ug+1)}\right]$$

$$D_{DERi} = [D_{DERi}(1), D_{DERi}(2), \ldots, D_{DERi}(t), \ldots, D_{DERi}(T)];$$
$$i = 1, 2, \ldots, (ug + 1)\ D_{DERi} \in \{0, 1\}$$

$$D_{ESS} = \left[D_{ESS1}, D_{ESS2}, \ldots, D_{ESS(us)}\right]$$

$$D_{ESSj} = [D_{ESSj}(1), D_{ESSj}(2), \ldots, D_{ESSj}(t), \ldots, D_{ESSj}(T)];$$
$$j = 1, 2, \ldots, us\ D_{ESSi} \in \{0, 1\} \tag{5}$$

where $D_{DERi}(t),\ D_{ESSj}(t)$ are the state vectors which demonstrate the ON or OFF states of all DERs and ESS units at hour t, respectively.

3.2. System constraints

Under the consideration of DERs and main grid characteristics, RT-EMS should ensure the steady state security and reserve capacity margin for MG when participating in the power market. Accordingly, the following constraints are defined and applied to the optimization model of MG.

3.2.1. Load power balance

This constraint states that the summation of load demand power $P_L(t)$ must be equal to the summation of DERs power $P_{DERi}(t)$, and the main grid net power $(P_{gs}(t) - P_{gr}(t))$ at hour t. The mathematical expression for such constraint can be written as follows:

$$\sum_{l=1}^{ul} P_L(t) - \left(\sum_{i=1}^{ug} P_{DERi}(t) + P_{gr}(t) - P_{gs}(t)\right) = 0 \tag{6}$$

where ul is the total number of load levels.

3.2.2. Emission constraint

To improve the public image, DERs and the main grid should work within acceptable emission limits which depend on the emission standards reference guide of each country [21]. This part of the work presents the constraint for the emissions caused by DER units. The three most important gaseous emissions considered in the current work are: carbon dioxide (CO_2) and the pollutants sulfur dioxide (SO_2) and nitrogen oxides (NO_x). It is assumed that each unit should not exceed the maximum significant emission rate for each gas in kg during one hour of operation. These limits are designed to regulate air emissions from electrical power production at MG and the utility grid. Such limits can be written as follows:

$$E_{CO_{2_{DERi}}} P_{DERi}(t)\ or\ E_{CO_{2_g}}(t) P_g(t) \leqslant \mathrm{E}^{\max}_{CO_2}(t) \tag{7}$$

$$E_{NO_{X_{DERi}}} P_{DERi}(t)\ or\ E_{NO_{X_g}}(t) P_g(t) \leqslant \mathrm{E}^{\max}_{NO_X}(t) \tag{8}$$

$$E_{SO_{2_{DERi}}} P_{DERi}(t)\ or\ E_{SO_{2_g}}(t) P_g(t) \leqslant \mathrm{E}^{\max}_{SO_X}(t) \tag{9}$$

$$P_g(t) = P_{gs}(t) - P_{gr}(t) \tag{10}$$

$\mathrm{E}^{\max}_{CO_2}$, $\mathrm{E}^{\max}_{NO_X}$ and $\mathrm{E}^{\max}_{SO_2}$ represent the maximum emission rates of CO_2, NO_X and SO_2 respectively for each unit in kg at time t. $E_{CO_{2_{DERi}}}$, $E_{NO_{X_{DERi}}}$, and $E_{SO_{2_{DERi}}}$ are the emission factors of carbon dioxide, nitrogen oxides and sulfur dioxide emission delivered by each DER in kg/kW h. $E_{CO_{2_g}}$, $E_{NO_{X_g}}$, and $E_{SO_{2_g}}$ are the emission factors of carbon dioxide, nitrogen oxides and sulfur dioxide emission delivered by the utility grid in kg/kW h respectively [21]. The rest of the above parameters are defined in Section 3.4. The mathematical formulation of the net emission of carbon dioxide, nitrogen oxides, and sulfur dioxide during 24 h of operation are expressed in Eqs. (12), (13), and (14) respectively.

$$f_2(x) = \sum_{t=1}^{T} \left\{ \begin{array}{c} \sum_{i=1}^{u_g} D_{DERi}(t) P_{DERi}(t) E_{CO_{2_{DERi}}}(t) \\ + \\ P_g(t) E_{CO_{2_g}}(t) \end{array} \right\} \tag{11}$$

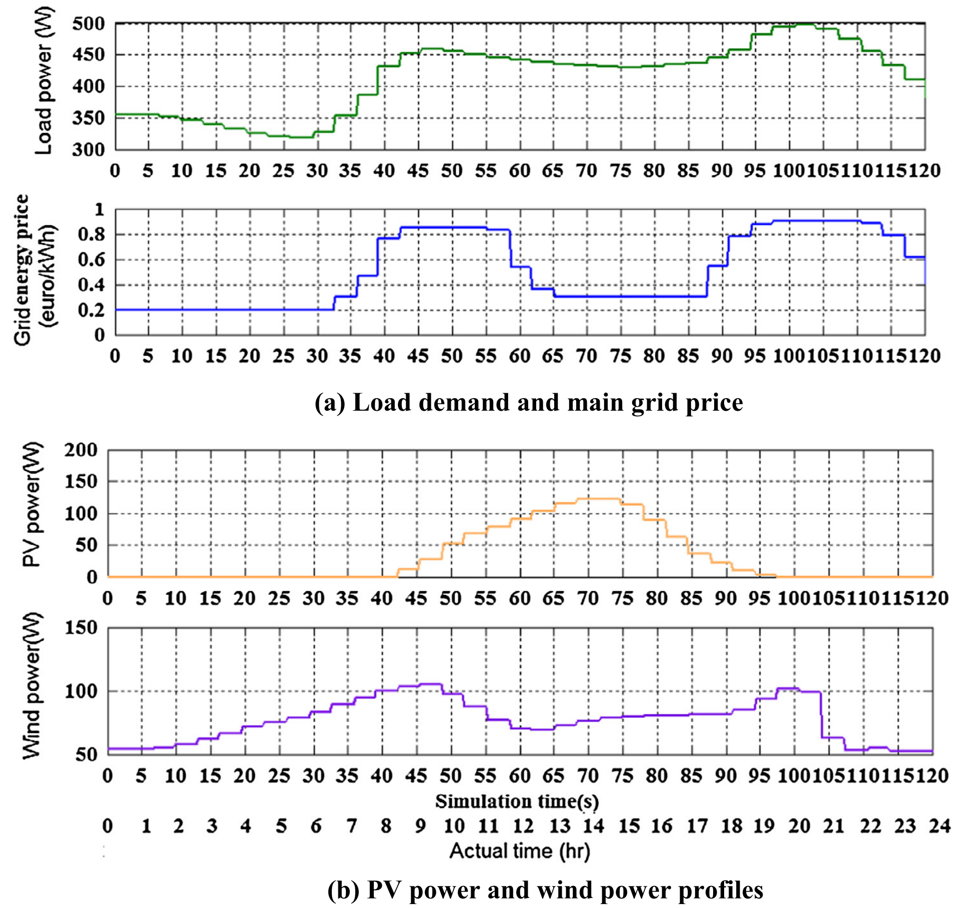

Fig. 3. (a) Load demand and main grid price. (b) PV power and wind power profiles.

Table 1
Power capacity, LCOE [17] and DERs emission factors [5].

MG parameters	PV	FC	Wind	Main grid
LCOE (€/kW h)	0.8	0.38	0.7	As in Fig. 3
CO_2 (kg/kW h)	0	0.230	0	0.368
SO_2 (kg/kW h)	0	0.0028	0	0.0002
NO_X (kg/kW h)	0	0. 0075	0	0. 0008
Min power (W)	0	10	10	10
Max power (W)	130	150	120	400

$$f_3(x) = \sum_{t=1}^{T} \left\{ \begin{array}{c} \sum_{i=1}^{u_g} D_{DERi}(t) P_{DERi}(t) E_{SO_{2_{DERi}}}(t) \\ + \\ P_g(t) E_{SO_{2_g}}(t) \end{array} \right\} \tag{12}$$

$$f_4(x) = \sum_{t=1}^{T} \left\{ \begin{array}{l} \sum_{i=1}^{u_g} D_{DERi}(t) P_{DERi}(t) E_{NO_{X_{DERi}}}(t) \\ + \\ P_g(t) E_{NO_{X_g}}(t) \end{array} \right\} \tag{13}$$

The mathematical description of the carbon dioxide emission factors can be stated as follows:

$$E\_CO_{2_{DERi}}(t) = \left[E\_CO_{2_{DERi}}(1), E\_CO_{2_{DERi}}(2), \ldots, E\_CO_{2_{DERi}}(T)\right] \tag{14}$$

$$E\_NO_{x_{DERi}}(t) = [E\_NO_{x_{DERi}}(1), E\_NO_{x_{DERi}}(2), \ldots, E\_NO_{x_{DERi}}(T)] \tag{15}$$

$$E\_SO_{2_{DERi}}(t) = [E\_SO_{2_{DERi}}(1), E\_SO_{2_{DERi}}(2), \ldots, E\_SO_{2_{DERi}}(T)] \tag{16}$$

3.2.3. Supply constraints

For stable operation, each DER unit is subject to the technical limits which include the upper and lower bounds as follows:

$$\mathrm{P}_{\mathrm{DERi}}^{\mathrm{min}}(\mathrm{t}) \leqslant P_{DERi}(t) \leqslant \mathrm{P}_{\mathrm{DERi}}^{\mathrm{max}}(\mathrm{t}) \quad i = 1, 2, 3, \ldots, ug \tag{17}$$

where $\mathrm{P}_{\mathrm{DERi}}^{\mathrm{min}}(\mathrm{t}), \mathrm{P}_{\mathrm{DERi}}^{\mathrm{max}}(\mathrm{t})$ are the minimum and maximum operating powers of each DER at time t.

3.3. System inputs

This section presents a full description for the MG system inputs such as: load demand, grid tariff, PV and wind power profiles which are shown in Fig. 2. The forecasting model used to predict the load, PV and wind power profiles is regenerated from the model derived in [22]. This model is implemented based on the historical data which are obtained from the French Transmission Network of Electricity (RTE) [23].

Fig. 3a shows the average daily electricity load profile and main utility energy price during one typical day in winter season. It is well known that the electricity demand varies according to some factors such as the time of day, time of year, geographical location and climate [24].

Demand variation is reflected in main grid market fare and/or supply contracts that ensure high energy price when demand is high and less when it is low. This price is for general residential usage and may be suitable for customers who use most of their electricity during off-peak times. In this work, it is assumed that energy prices during peak hours are a bit higher than usual [25] to show the power exchange between the MG and the utility in grid-connected mode.

Fig. 3b shows the wind and PV power profiles. These power profiles are obtained from RTE- France during one typical day in winter then multiplied by a factor to be suitable for small scale power applications [23].

For all graphs, it is assumed that 5 s in the simulation time are equivalent to 1hour. So, the daily 24 h operation is represented by 120 s in the simulation time.

3.4. System parameters

This section presents supply power limits, operating cost, and emission factors for each DER during operating time.

3.4.1. Supply capacity power limits

Each generator has maximum limits for the output power during operating mode as listed in Table. 1.

Main grid units are assumed to work all the time with a power range between minimum and maximum limits. This assumption is used in our study for two reasons. The first reason is to stabilize and supplement intermittent sources of power such as wind and solar which are limited by geography, weather, and space constraints. The second reason is because the generation units of the main grid require a long period of time and high cost to heat up to operating temperature.

3.4.2. Supply cost and emission factors

In DER units, Levelized Cost of Electricity LCOE (€/kW h) is traditionally calculated by discounting the investment cost and operating/maintenance costs over the lifetime divided by the annual electricity production. The first row in Table 1 shows that the LCOE of each generation unit [25]. In this row, it can be noticed that the LCOE of PV plant is higher than all the other resources according to the high investment and the financing costs in the considered country [26].

The second, third, and fourth row of the table present the total CO_2, SO_2, and NO_x emissions of each DER unit. It is assumed in this study that each generator unit should not exceed the maximum emission rate for each gas which considered as 0.15 kg ofCO_2, 9e−5 kg of SO_2, and 5e−4 kg of NO_X emissions during one hour of operation. These maximum rates vary from country to country according based on the emission standards reference guide of each country [21].

On the other hand, it is assumed that 60% of the utility grid power production is coming from nuclear generation system (0 emission) while 40% is coming from a coal generation system (0.920 kg/kW h of CO_2, 0.0005 kg/kW h of SO_2, and 0.002 kg/kW h of NO_x) [5].

3.5. Optimization algorithm

To improve the performance of RT-EMSs, a robust and fast optimization algorithm is required to find the optimal allocation for each DER unit in real time. Therefore, in this paper the optimization problem is solved by using BPSO.

Particle swarm optimization was originally invented by Kennedy and Eberhart as admitted in [27]. PSO is one of the evolutionary optimization method inspired by nature. It is a relatively recent heuristic search method whose mechanics are inspired by the swarming or collaborative behavior of biological populations. In PSO algorithm, each feasible solution of the problem is called a particle which is specified by a vector containing the problem variables. Particles have memory and thus retain parts of their previous state. There is no restriction for particles to share the same point in belief space, although their individuality is protected. Each particle adjusts its own position toward its previous experience and toward the best previous position obtained in the swarm [28]. Memorizing its best own position establishes the particle's experience implying a local search along with global search emerging from the neighboring experience or the experience of the whole swarm [29]. The particles fly through the n dimensional domain space of the function to be optimized. The state of each particle is represented by its position $X_i = (X_{i1}, X_{i2}, \ldots, X_{in})$ and velocity$V_i = (V_{i1}, V_{i2}, \ldots, V_{in})$. The states of the particles are updated. The three key parameters of particle swarm optimization

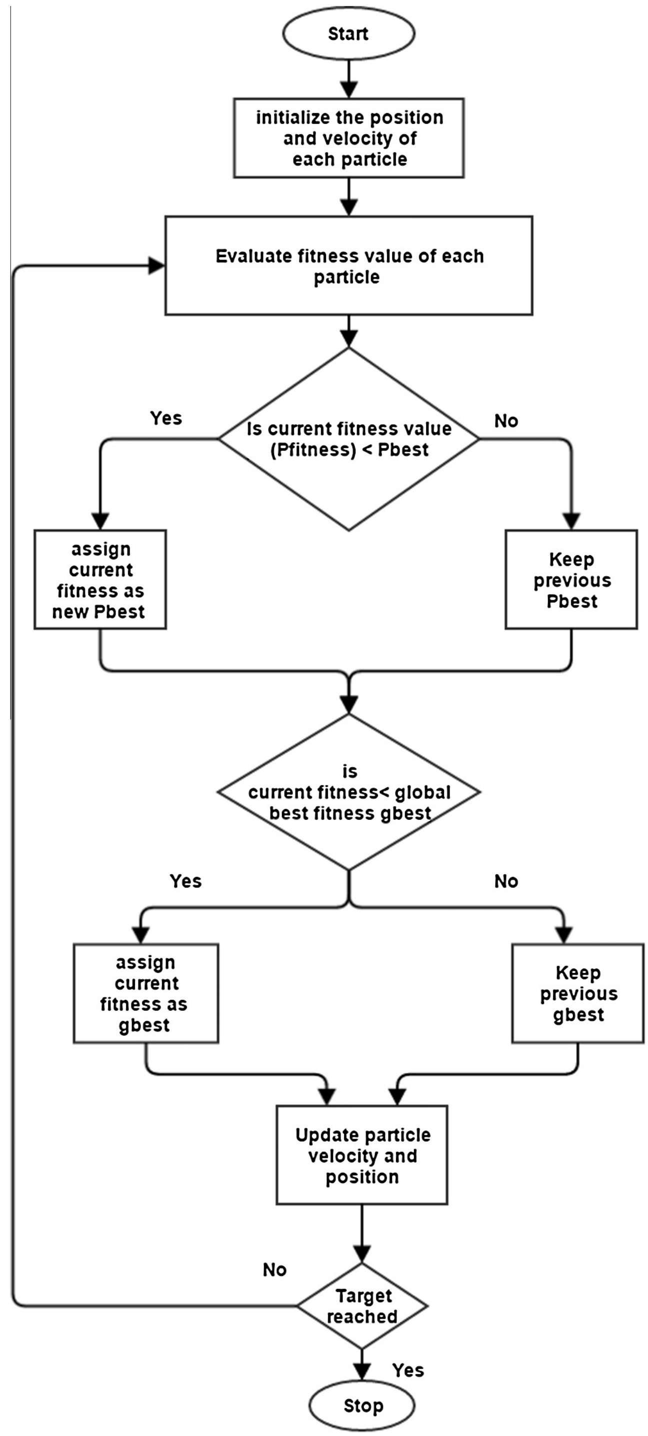

Fig. 4. BPSO flowchart.

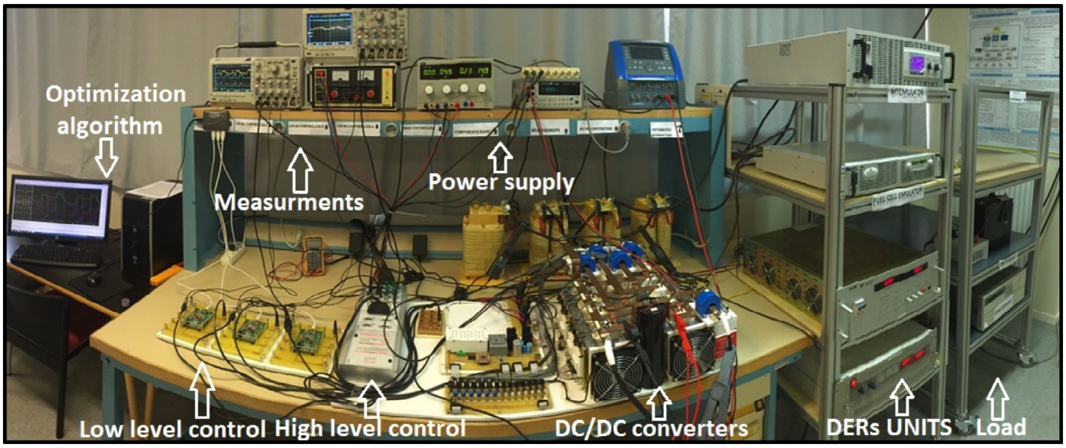

Fig. 5. The experimental test bench.

Table 2
Boost converters Module Parameters [33].

DC-DC boost converter parameters	Values
Inductance (l)	2 mH
Inductor resistance (R_l)	40 mΩ
Capacitance (C)	6800 µF
Capacitor resistance (R_c)	24 mΩ
Switching frequency (f_s)	10 kHz

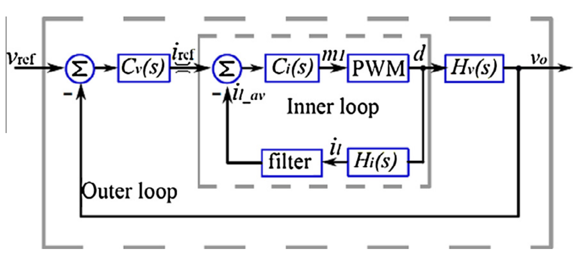

Fig. 6. Main control scheme for the main utility grid.

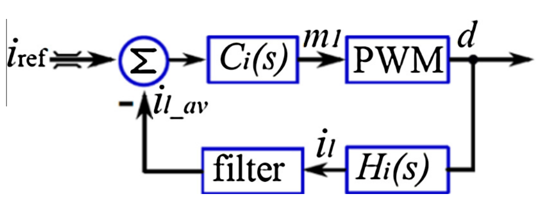

Fig. 7. Main control scheme for PV, WT and FC.

algorithm can be found in the velocity update equation as in Eq. (19). The first component is the inertial weight coefficient, which allows balancing the local search and the global search through the determination of the contribution rate of a particle's previous velocity to its velocity at the current time step. An elevated value of this coefficient facilitates a global search, on the contrary local search is facilitated [30]. The second component is the momentum component, which is called the cognitive component and its acceleration factor (c1) responsible to control how much the particle heads toward its personal best position. The third component is the social component, which draws the particle toward swarm's best ever position based on the acceleration constant (c_2). At the beginning of the algorithm, a group of particles is randomly initialized in the search space. Each particle makes use of its memory and flies through the search space for obtaining a better position than its current one. In its memory, a particle memorizes the best experience found by itself (p_{best}) as well as the group's best experience (g_{best}) [31]. The position of each particle in that space is achieved using the following equations:

$$v_i^{k+1} = v_i^k w^k + c_1 r_1 (p_{best}^k - x_i^k) + c_2 r_2 (g_{best}^k - x_i^k) \tag{18}$$

$$x_i^{k+1} = (x_i^k - v_i^{k+1}) \tag{19}$$

where $v_i^k$and x_i^k are the components in dimension d of the ith particle velocity and position in iteration k respectively. c_1 and c_2 are considered the cognitive and social components where r_1 and r_2 are the real numbers randomly generated between [0 and 1]. w is the inertia weight coefficient. p_{best} is the best position achieved so far by a particle i where g_{best} is the best position found by the neighbors of particle i. Basically, the standard PSO consists of three steps as presented in Fig. 4. Regarding to BPSO used in this paper, the population size = 50, the inertial weight coefficient = 1, initial and final social parameters are equal to 0.5 and 2.5 respectively. The initial and final cognitive parameters are 2.5 and 0.5. Finally, the construction fact was set to 1 and the minimum and maximum velocity were set to −4 and 4 respectively.

4. Hardware implementation

In order to implement the RT-EMS, an experimental test bench, shown in Fig. 5, has been designed in our laboratory. Three DC programmable power supplies, i.e., EA-SI8080 and GEC5000, are used to emulate the typical power profiles of FC, PV, and WT. In addition, three phase rectifier module suitable for laboratory scale is used to rectify the AC power of the main grid. Other than that, four conventional DC-DC boost converters are connected in parallel in order to integrate all DER units and main grid to the MG's DC-bus, where its voltage is regulated at 50 V. The switching device, skm121ar from semikron, is used for the DC-DC boost converters modules to achieve small switching and conduction losses. The parameters of the boost converters are listed in Table. 2.

The programmable electronic load (N3300A) is used to emulate load demand power profile. The electronic load has the flexibility to test a wide range of loading conditions with fast operation and accurate programming. MTX1032 and FLUKE 80i-110s are used respectively as differential voltage and current probes to measure the voltage and current signal where the power profiles were recorded by using Tek-DPO2000.

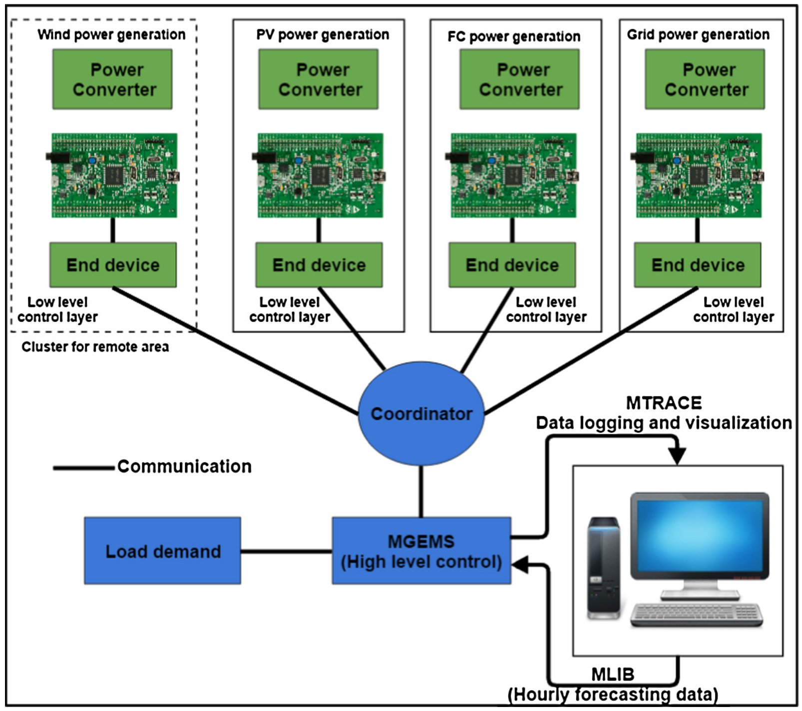

Fig. 8. MLIB/MTRACE network topology.

4.1. Control design and implementation

The control system is divided based on the speed and functions on low and high level control layers.

4.1.1. Low level control (local control) design

The low level control layer, local controller, generates the necessary Pulse Width Modulation (PWM) signals to the DC-DC converters based on advanced lead lag compensator (ALLC), which is implemented on the ARM Cortex M4 processor. This control layer performs fast computation for the control action and protection function which requires high bandwidth with a fast and predictable time response. The DSP extension for ARM Cortex M4 assists in fast computation of the control output. The built in dedicated PWM module and analog to digital converters with direct memory access make it possible to acquire analog feedback signals with a fast sampling rate while operating on fast switching frequencies. The STM32f407vgt6 processor running at 160 MHz was used for the embedded implementation of the control layer. This kind of high speed controllers is needed to generate PWM carriers with very high switching frequency in order to decrease the size of the output capacitor and inductor. In addition, it is necessary for auto-tuning process of the controller parameters in order to improve the dynamic performance.

In this implementation, the voltage and current ALLC are employed during transient and steady-state conditions for controlling the boost converter of main utility grid as shown in Fig. 6. On the other hand, the current ALLC shown in Fig. 7 is employed for PV, wind and FC.

The controllers are designed based on the Small Signal Model (SSM) using frequency response techniques. The SSM for the boost converters is derived in details in [32].

The equation of current and voltage control can be written as follows:

$$C_i(s) = k_{ci}\frac{(s+zi)}{s(s+pi)} \tag{20}$$

$$C_v(s) = k_{cv}\frac{(s+zv)}{s(s+pv)} \tag{21}$$

where $C_v(s)$ is the voltage compensator and $C_i(s)$ is the current compensator that assures cancellation of the static error and high bandwidth. A pole at the origin is considered as an integral action and provides a very high gain at low frequencies. Moreover, the pole-zero pairs (pi, zi) for current controller and (pv, zv) for voltage controller aim to reduce the phase shift between the frequency of the two plant zeros and the frequency of two plant poles.

$$zi = w_{cni}\sqrt{\frac{1-\sin\emptyset_{mdi}}{1+\sin\emptyset_{mdi}}},\quad pi = \frac{zi}{\sqrt{\frac{1-\sin\emptyset_{mdi}}{1+\sin\emptyset_{mdi}}}} \tag{22}$$

$$zv = w_{cnv}\sqrt{\frac{1-\sin\emptyset_{mdv}}{1+\sin\emptyset_{mdv}}},\quad pv = \frac{zv}{\sqrt{\frac{1-\sin\emptyset_{mdv}}{1+\sin\emptyset_{mdv}}}} \tag{23}$$

where w_{cni}andw_{cnv} are the new crossover frequencies of the current inner loop and the voltage outer loop, respectively. The compensator phase margin of the current and the voltage controller are abbreviated as $\emptyset_{mdi}$ and $\emptyset_{mdv}$, respectively. k_{ci} is the current controller gain where k_{vi} is the voltage controller gain which can be calculated as the following:

$$k_{ci} = |\frac{1}{\mathrm{Ti(S)}}|\ at\ w = w_{cni} \tag{24}$$

$$k_{vi} = |\frac{1}{\mathrm{Tv(S)}}|\ at\ w = w_{cnv} \tag{25}$$

where $T_i(s)$, $T_v(s)$ are the open loop transfer functions for the inner and outer loop, respectively.

$$T_i(s) = C_i(s)H_i(s) \quad \text{for the inner loop} \tag{26}$$

$$\mathrm{T_v(s)} = \frac{\mathrm{C_v(s)C_i(s)H_v(s)}}{1+\mathrm{C_i(s)H_i(s)}} \quad \text{for the outer loop} \tag{27}$$

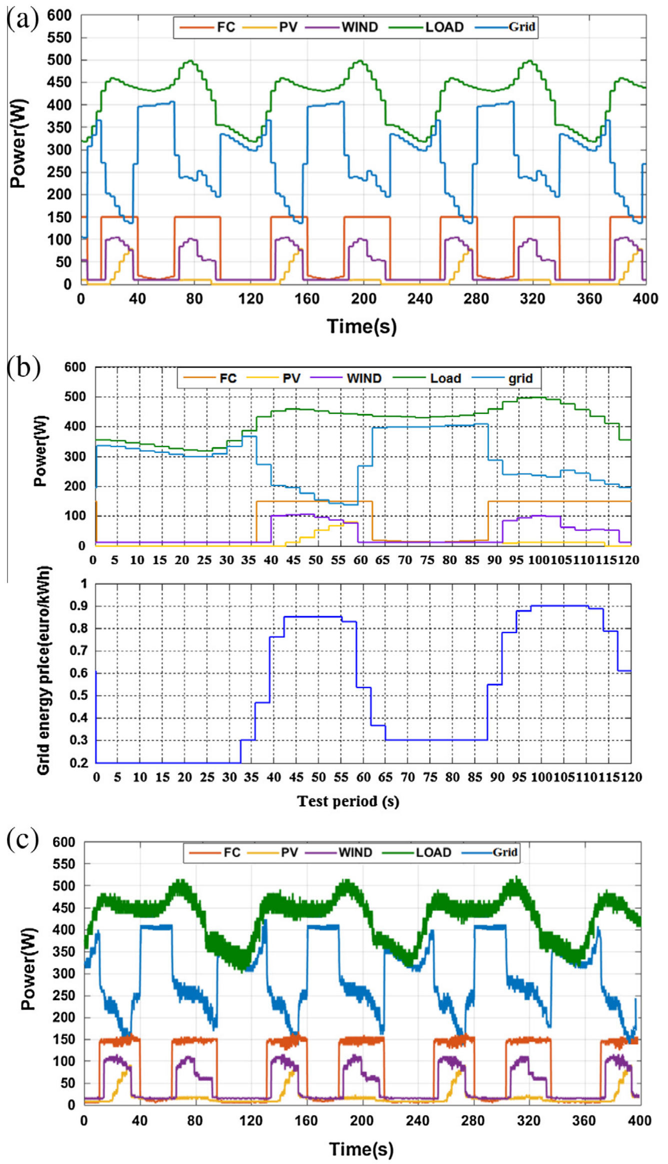

Fig. 9. (a) Optimal power allocation based on BPSO of scenario 1. (b) Optimal power allocation for one day of simulation which represent 120 s in the test period. (c) Actual power profiles of scenario 1. (d) DC link voltages of scenario 1. (e) Total cost cariation of scenario 1.

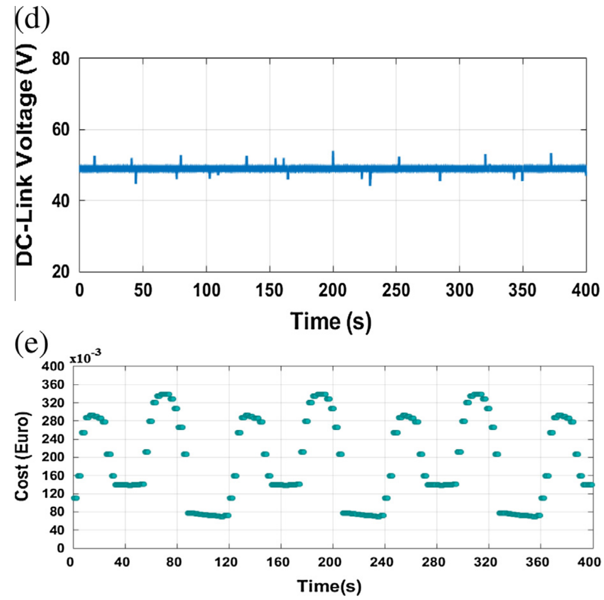

Fig. 9 (*continued*)

where $H_i(s)$, $H_v(s)$ are the current and voltage transfer functions of DC-DC boost converters, which can be found in [32,33].

For the main utility grid local controller, the crossover frequency of the current-loop is selected to be 1.2 times of the plant crossover frequency, with a phase margin equal to 50°. To avoid the interaction between subsystems, low bandwidth control is used for the voltage outer loop which has a crossover frequency 1.1 times of crossover frequency one and a phase margin equal to 65°. For the remaining local controllers, the crossover frequency of the current-loop is selected to be 1.2 times of the plant crossover frequency.

4.2. High level control design

The high level control layer is the optimization layer which generates the power reference for the distributed resources to optimize the cost and emissions.

To guarantee real-time performance, the optimization code is running in a dSPACE 1104 embedded controller. This control layers receive measurements from the low level controllers, load demand variation and calculate the power reference for each source taking into account the economical and environmental impacts. The power reference is sent back to the low level controller to control the DC-DC converters through wired communication network. The forecasted data for load and available energy is exchanging with the RT-EMS through the dSPACE Real-time MLIB/MTRACE libraries as shown in Fig. 8.

The MLIB/MTRACE are considered as new tools to be used in real time energy management systems. The function of these two libraries is to provide direct access from MATLAB scripts to runtime data of the application running on a dSPACE board in real time, without interrupting the process [19]. MTRACE provides real-time data capture for the system variables such as load demand, available wind power, and grid tariff for logging and visualization, while MLIB writes the BPSO's output values back to the dSPACE processor memory without interrupting the operation.

In this study, BPSO worked to run the optimization code and to take decision every 1 s where the sampling time of the load variation, grid energy price and the available power profile of non dispatchable was set to 3.25 s. Thus, the update rate of the unit dispatch command will be fast enough to follow the sudden changes of load and intermittent generators in real-time. In addition, it is assumed also in the practical results that each 5 s during operating test period is equivalent to 1 h in the real-time operation.

5. Experimental results

This section presents the experimental results which are obtained based on the proposed RT-EMS and its wired communication and control systems. The optimization results of the MG system are evaluated using BPSO during 120 s. The optimization model takes into account the variation of the load demand profile, main grid energy price, and PV and wind power variation during the operating time. Furthermore, it is considered that all generators are either in the MG or in the main grid in operating mode and the algorithm is intended to choose the optimum mode according to the cost and emission objective functions. Three

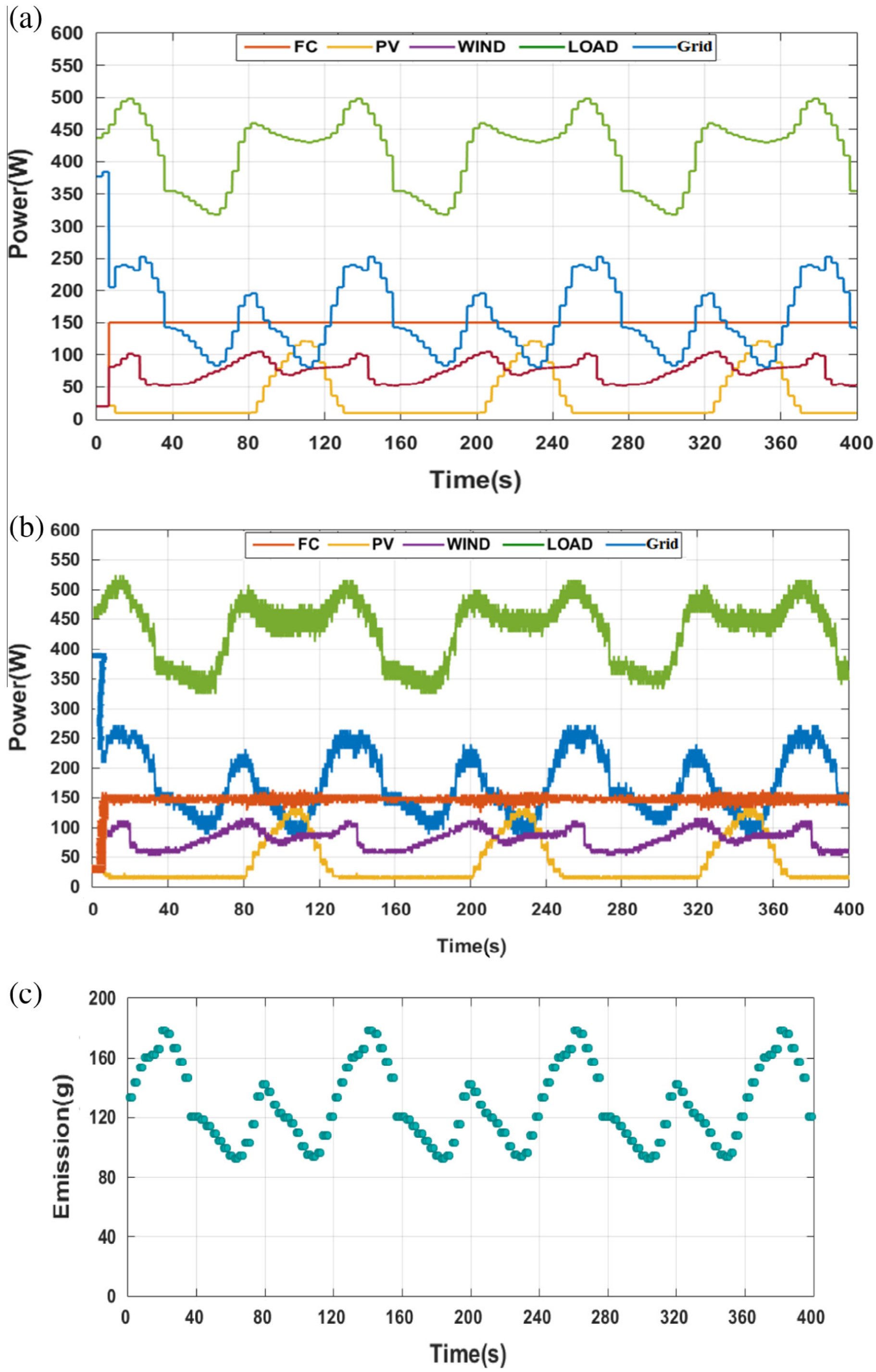

Fig. 10. (a) Optimal power allocation based on BPSO of scenario 2. (b) Actual power profiles of scenario 2. (c) Total emission variation of scenario 2.

scenarios are proposed to test the efficient performance of the proposed RT-EMS.

5.1. Scenario 1

In this scenario, the optimization results of the MG system are evaluated to achieve the economical solution without taking into account the environmental solution.

In Fig. 9a, the optimal power allocation generated by BPSO (Reference values) are presented for all DERs during 400 s which represents more than 3 days of operation. Fig. 9b is used to show a full description for one operating day of simulation. It is clear from this figure that all DERs in MG system are aimed to verify load profile requirements.

In the first period of operation, from 0 s to 39 s, a major part of the load is supplied by the main grid output power due to the decrease of its energy price compared to the other DERs as well as the reduction of load demand. Over the next operating period, from, a major part of the load is supplied by FC, PV, and wind due to the energy price of their units are lower compared to the main grid as well as the growth of the load demand. During this period of the day, the MG can sell some power to another MG or

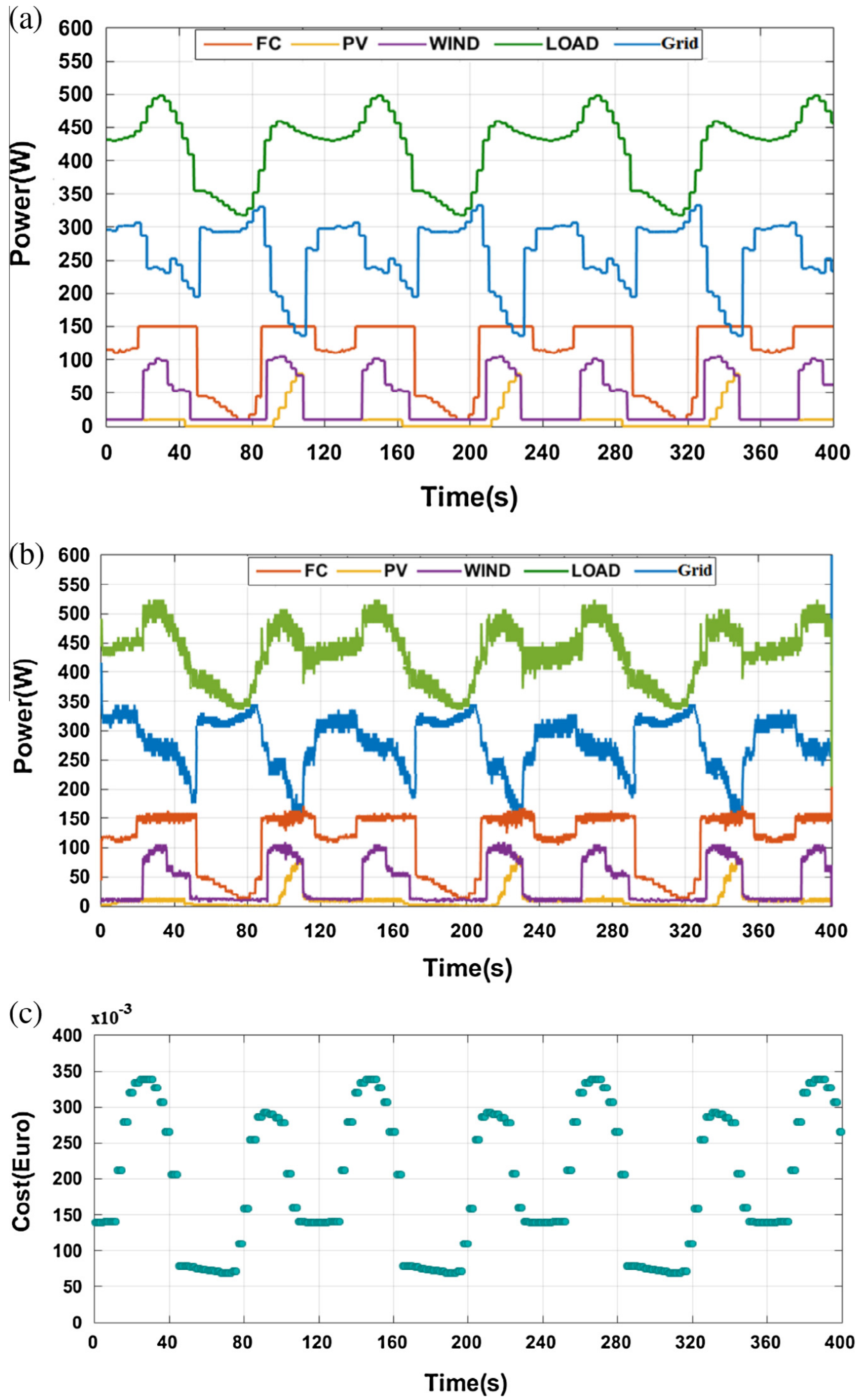

Fig. 11. (a) Optimal power allocation based on BPSO of scenario 3. (b) Outputs of the BCM of scenario three. (c) Total cost variation of scenario 3.

to the main grid if the generated power exceeds the load demand. In another scenario, islanded operated mode, this power can be used to charge ESS when the load demand and energy price are low, and the discharge action can be postponed when the load demand reaches its peak values.

Fig. 9c shows the DC-DC boost converters modules (BCM) output power profile of main grid, FC, PV, wind power profiles and load demand. As it can be observed, the real output power produced by BCM is tracking very well the RT-EMS references power profiles which are shown in Fig. 9a. It is also clear from the figures that the total of the DERs power can meet the active power of load demand.

In Fig. 9d, the profile of the DC-link voltage is presented. The DC-link voltage is well regulated at 50 V with voltage ringing equal to 10% during the continuous variation of DERs power production and load demand power consumption. A new control scheme is proposed in [33] in order to reduce the voltage ringing during load demand and supply variation.

Fig. 9e shows the total cost during test period. It is clear from the results that the total cost is tracking the load demand profile.

At t = 70 s, the maximum total cost is recorded according to the increasing of DERs power production to satisfy load requirements.

In this work, the optimization process occurred every 1 s to achieve high efficient performance for the RT-EMS. In addition, BPSO reaches the minimum cost after 30 iterations which reflect the fast processing speed of the algorithm.

5.2. Scenario 2

In this scenario, the optimization problem is solved also based on the power of BPSO taking into account the environmental solution without considering the economical one.

Fig. 10a shows the outputs of the RT-EMS based on BPSO. It is clear from the figure that a major part of the load is supplied by renewable energy such as FC, PV, and wind according to their low emission factors. Therefore, the main grid generates power equals to the difference between renewable energy power and load demand power. Fig. 10b shows the BCM output power profiles of the main grid, FC, PV, wind and load demand profile. It can be observed from the figure that the real output power produced by DERs boost converters is tracking the EMS's reference power profiles.

Fig. 10c shows the variation of total emission during test period. It is noted from the figure that the total emission has the same profile as load demand. At t = 20 s, the maximum emission level is recorded according of the increasing of DERs power production at this instant. In this scenario, the BPSO reached the minimum emission level for every trail after 27 iterations.

5.3. Scenario 3

In the third scenario, the same optimization problem is solved based BPSO taking into account the economical solution and environmental constraints. All the required data for solving the optimization problem as well as the technical specification of the MG real time market prices remain unchanged.

The results of the mentioned optimization problem are given in Fig. 11a. Further, Fig. 11b presents the BCM output power profiles of the main grid, FC, PV, wind power and load demand profiles.

It is observed in the first interval of the test (from 20 s to 50 s), a major part of the load is supplied by the main FC and Wind generator because the energy price of their units are lower compared to the main grid. Power generation from PV system is measured equal to zero according to the absence of solar radiation during this period of the test.

In the next interval, the major part of load is supplied by main grid. It is worthy to note that the output power from main grid in this scenario is limited to 320 W. The reason behind this fact is related to the CO_2 emission constraints. It can be observed also from the two figures that the actual power profiles of all DER units are following the EMS's reference power.

Fig. 11c shows the cost optimization process during the test interval in order to minimize total cost during operating hours taking into account emission constraints as well as to meet load requirements. As a comparison, the total cost in this scenario is recorded at peak load demand higher than scenario one. The reason behind this fact is related to the limitation of grid maximum power production according to emission constraints.

In scenario one, BPSO is succeed to reach the minimum cost after 30 iteration where in this scenario after 40 iterations. The difference is related to the complexity of the optimization problem in this scenario compared to scenario one.

6. Conclusion

In this paper, an effective and advanced Real-Time Energy Management System (RT-EMS) is proposed for MG operation in order to achieve the optimal power allocation for the aforementioned DERs. The optimization model considered two inconsistent objectives where the total MG operating costs and the associated pollutant emission were analyzed. Constraint functions were added to the optimization problem to reflect some of the additional considerations often found in a small-scale generation system. The optimization problem of the proposed RT-EMS is solved using Binary Particle Swarm Optimization algorithm (BPSO). To evaluate the performance of RT-EMS along with its optimization algorithm, three different scenarios were introduced and analyzed for a typical MG testbed. The simulation and experimental results for all scenarios proved that the proposed RT-EMS based on BPSO is able to provide robust and efficient solution for MG power systems which are working in island and grid connected mode.

In our future work, we will consider the demand response programs and the participation of plug-in electric vehicles in MG power systems. In such systems, MG can work with a high level of flexibility avoiding the significant increase of consumption in peak periods. In addition, we will take into account a new strategy for the prediction of PV and wind power profiles. The optimization model of this MG therefore becomes significantly different from the one we considered in this paper and worth further studies.

References

[1] Lidula NWA, Rajapakse AD. Micro-grids research: a review of experimental micro-grids and test systems. Renew Sustain Energy Rev 2011;15:186–202.
[2] Huang J. A review on distributed energy resources and micro-grid. Renew Sustain Energy Rev 2008;12:2472–83.
[3] Taha S. Recent developments in micro-grids and example cases around the world—a review. Renew Sustain Energy Rev 2011;15:4030–41.
[4] Alavi Seyed Arash, Ahmadian Ali, Aliakbar-Golkar Masoud. Optimal probabilistic energy management in a typical micro-grid based-on robust optimization and point estimate method. Energy Convers Manage 2015;95:314–25.
[5] Aghajani GR, Shayanfar HA, Shayeghi H. Presenting a multi-objective generation scheduling model for pricing demand response rate in micro-grid energy management. Energy Convers Manage 2015;106:308–21.
[6] Bruni G, Cordiner S, Mulone V, Rocco V, Spagnolo F. A study on the energy management in domestic micro-grids based on model predictive control strategies. Energy Convers Manage 2015;102:50–8.
[7] Choudar Adel, Boukhetala Djamel, Barkat c Said, Brucker Jean-Michel. A local energy management of a hybrid PV-storage based distributed generation for microgrids. Energy Convers Manage 2015;90:21–33.
[8] Tazvinga Henerica, Zhu Bing, Xia Xiaohua. Optimal power flow management for distributed energy resources with batteries. Energy Convers Manage 2015;102:104–10.
[9] Derakhshandeh SY, Masoum AS, Deilami S, Masoum MAS, Golshan MEH. Coordination of generation scheduling with PEVs charging in industrial microgrids. IEEE Trans Power Syst 2013;28:3451–61.
[10] Vandoorn T, Vasquez J, De Kooning J, Guerrero J, Vandevelde L. Micro-grids: hierarchical control and an overview of the control and reserve management strategies. IEEE Trans Ind Electron Mag 2013;7(4):42–55.
[11] Elsied M, Oukaour A, Gualous H, Hassan R, Amin Amr. An advanced energy management of micro-grid system based on genetic algorithm. Istanbul: ISIE IEEE; 2014.
[12] Karavas Christos-Spyridon, Kyriakarakos George, Arvanitis Konstantinos G, Papadakis George. A multi-agent decentralized energy management system based on distributed intelligence for the design and control of autonomous polygeneration micro-grids. Energy Convers Manage 2015;103:166–79.
[13] Logenthiran T, Srinivasan D, Khambadkone AM, Raj TS. Optimal sizing of an islanded micro-grid using evolutionary strategy. In: International conference on probabilistic methods applied to power systems (PMAPS). Singapore: IEEE; 2010.
[14] Colson CM, Nehrir MH, Wang C. Ant colony optimization for micro-grid multi-objective power management. In: Power systems conference and exposition. PSCE '09, WA, Seattle.
[15] Elsied M, Oukaour A, Gualous H, Hassan R, Amin Amr. Gestion de l'énergie et optimisation du système multisources basée sur l'algorithme génétique. SGE'14, July 2014.
[16] Elsied M, Oukaour A, Gualous H, Hassan R. Energy management and optimization in micro-grid system based on green energy. Energy J 2015;84(May):139–51.

[17] Marzband M, Sumper A, Ruiz Alvarez A, Domnguez Garca JL, Tomoiaga B. Experimental evaluation of a real time energy management system for stand-alone micro-grids in day-ahead markets. Appl Energy 2013;106:365–76.
[18] Marzband Mousa, ghadimi Majid, sumper Andrea, luis Jose. Experimental validation of a real time energy management system using multi-period gravitational search algorithm for micro-grid in islanded mode. Appl Energy 2014;128:164–74.
[19] dSPACE User's Guide Reference Guide. RTI 31: Real-time interface to SIMULINK. dSPACE GmbH; 2012.
[20] Mohamed Faisal A. Online management genetic algorithms of micro-grid for residential application. Energy Convers Manage 2012;64:562–8.
[21] European emission standards. Available from <https://en.wikipedia.org/wiki/Emission_standard>.
[22] Mohamed Ahmed, Mohammed Osama. Real-time energy management scheme for hybrid renewable energy systems in smart grid applications. Electric Power Syst Res 2013;96:133–43.
[23] RTE Electrical in France; 2016. Available from: <http://www.rte-france.com/en/eco2mix/eco2mix>.
[24] Marszal-Pomianowska Anna, Heiselberg Per, Kalyanova Larsen Olena. Household electricity demand profiles – a high-resolution load model to facilitate modelling of energy flexible buildings. Energy Build 2016;103:487–501.
[25] Eurostat. Electricity prices by type of user; 2015. <http://epp.eurostat.ec.europa.eu/tgm/table.do?tab=table&init=1&language=en&pcode=ten00117&plugin=1>.
[26] Breyer Christian. PV LCOE in Europe 2014-30 Technical report, 2016.
[27] García-Triviño P, Gil-Mena AJ, Llorens-Iborra F, García-Vázquez CA, ernández-Ramírez LM, Jurado F. Power control based on particle swarm optimization of grid-connected inverter for hybrid renewable energy system. Energy Convers Manage 2015;91:83–92.
[28] Behnood A, Gharavi H, Vahidi B, Riahy GH. Optimal output power of not properly designed wind farms, considering wake effects. Int J Electr Power Energy Syst 2014;63:44–50.
[29] Tahani M, Babayan N, Astaraei FR, Moghadam A. Multi objective optimization of horizontal axis tidal current turbines, using meta heuristics algorithms. Energy Convers Manage 2015;103:487–98.
[30] Chao KH. An extension theory-based maximum power tracker using a particle swarm optimization algorithm. Energy Convers Manage 2014;86:435–42.
[31] Lee KH, Kim W. Performance comparison of particle swarm optimization and genetic for inverse surface radiation problem. Int J Heat Mass Transf 2015;88:330–7.
[32] Elsied M, Salem A, Oukaour A, Gualous H, Chaoui H, Youssef FT, et al. Efficient power-electronic converters for electric vehicle applications. In: IEEE-vehicular power and propulsion conference 2015', Montreal, Canada, 19-22 Oct.
[33] Ayoubi Y, Elsied M, Oukaour A, Chaoui H, Slamania Y, Gualous H. Four-phase interleaved DC/DC boost converter interfaces for super-capacitors in electric vehicle application based on advanced sliding mode control design 6th International conference of fundamentals and development of fuel cells. Electric Power Syst Res 2016;134:186–96.